Article:

The neuronal ceroid lipofuscinosis protein Cln7 regulates neural development from the post-synaptic cell.

Kyle J. Connolly* [1], Megan B. O'Hare* [2], Alamin Mohammed* [1], Katelyn M. Aitchison[1], Niki C. Anthoney[1], Amy L. Roberts[1], Matthew J. Taylor [1], Bryan A. Stewart[3,4], Richard I. Tuxworth# [1,2] and Guy Tear# [2]

1. Institute of Cancer and Genomic Sciences
University of Birmingham
Birmingham
B15 2TT
UK

2: Department of Developmental Neurobiology
King's College London
New Hunt's House
London
SE1 1UL
UK

3: Department of Biology
University of Toronto Mississauga
Mississauga, ON
L5L 1C6
Canada

4. Department of Cell and Systems Biology
University of Toronto
Toronto, ON
M5S 3G5
Canada

* Equal contribution

co-senior and co-corresponding authors:
Guy.Tear@kcl.ac.uk
+44 (0)20 7848 6539

R.I.Tuxworth@bham.ac.uk
+44 (0)121 414 7046

ORCIDs:

MJT: 0000-0003-3055-4453
NCA: 0000-0003-3311-6328
KJC: 0000-0003-2425-3910
BAS: 0000-0003-2520-3632
RIT: 0000-0001-5697-6254
GT: 0000-0002-3114-7537

Running Title:
Cln7 regulates synapse development

Key words:
Neuronal ceroid lipofuscinosis, NCL, Cln7, retrograde signaling, neuromuscular junction, NMJ, *Drosophila*

Abstract

The development and maintenance of synapses requires co-ordination between the pre- and post-synaptic partners. We demonstrate that in *Drosophila,* Cln7, a MFS-domain transporter protein, is required to regulate normal synapse development. Cln7 is restricted to the post-synaptic muscle suggesting it is a novel component of a retrograde pathway regulating trans-synaptic communication. Loss of Cln7 leads to dysregulation of TORC activity, including excessive organismal growth and increased lipid storage phenotypes which are both dependent on TORC2 activity. Cln7 is mutated in late-infantile neuronal ceroid lipofuscinosis, an early-onset monogenetic neurodegenerative disorder, indicating that dysregulated TORC activity resulting in developmental synapse pathology may underpin the disease.

Introduction

The development and maintenance of synapses need to be precisely regulated to allow accurate flow of signals from the neuron to its target. Following circuit formation, synapse size continues to be adjusted and maintained through homeostatic mechanisms[1,2]. This plasticity of the synapse allows strengthening or weakening of connections and the accurate matching of presynaptic signal strength to the size of the postsynaptic target. Synapse homeostasis relies on anterograde and retrograde signaling across the synapse, which is mediated by a variety of signals[3,4]. Failure to form, maintain or adjust the synapse can lead to synapse failure or inefficiency leading to loss of neural function and degeneration. As such the synapse is a common target for neurodegenerative disease[4,5].

The *Drosophila* neuromuscular junction (NMJ) is a widely used genetically tractable model system to study synapse formation and homeostasis[6-8]. The *Drosophila* NMJ forms during embryonic development where the size of the pre-synaptic compartment is aligned with muscle size. During subsequent larval stages the muscle grows rapidly and synapse size expands to match this growth by increasing the number of neurotransmitter release sites (boutons), the amount of neurotransmitter release and the expression level of glutamate receptor subunits[9]. Retrograde signals such as the BMP ligand, glass bottom boat (gbb), are released from the post-synaptic side, activating a SMAD pathway in the neuron to influence

93 growth, reorganization of the cytoskeleton and the secretion of membrane[9]. The expansion
94 of the pre-synapse is also modulated via a variety of factors acting within neurons including
95 JNK signaling[10,11], levels of reactive oxygen species[12] autophagic pathways and regulators of
96 membrane traffic[4]. TORC-based mechanisms also act to co-ordinate postsynaptic glutamate
97 receptor levels in response to unknown trans-synaptic signals[13].

98 Many genes associated with human neurological conditions, including
99 developmental disorders and neurodegenerative diseases, have roles regulating NMJ
100 development[14,15]. Here we have investigated a role for the gene, *Cln7*, which is mutated in a
101 form of the childhood neurodegenerative disorder, neuronal ceroid lipofuscinosis (NCL)[16].
102 Evidence has accumulated in several models that loss of the *CLN* genes impacts on synapse
103 function, suggesting that they play a common role either within neurons or non-neuronal
104 cells to maintain function[17-19]. Recently, *Cln7* has been implicated in the activation of mTORC
105 signaling[20] and given the importance of TORC and autophagy for neuronal growth and
106 synapse homeostasis, we generated a *Drosophila Cln7* mutant to ask how these processes
107 might be affected in its absence. We identified a requirement for *Cln7* for normal neural
108 growth but, surprisingly, *Cln7* is restricted to the post-synaptic side of the NMJ where it
109 concentrates at the post-synaptic density. Autophagy and retrograde BMP signaling are
110 largely intact in *Cln7* mutants and instead the neurodevelopmental defect is likely due to
111 changes in TORC activity in the post-synaptic cell via interactions between Cln7 and Rheb.
112 This places Cln7 as a novel regulator of a retrograde TORC activity at the synapse and
113 highlights the importance of this pathway in neural development and disease.
114

115 **Results**

116 *Cln7 is localized in the basal sub-synaptic reticulum*

117 Disruption of the *Cln7* gene has been identified as the cause of a childhood
118 neurodegenerative disorder, late-infantile neuronal ceroid lipofuscinosis (LINCL/Cln7
119 disease)[16]. We had previously identified that the *Drosophila* Cln7 protein is expressed in the
120 body wall muscles that form the post-synaptic cells of the neuromuscular junction (NMJ),
121 where it concentrates at the post-synaptic density (PSD) (Fig. 1a)[21]. This distribution
122 suggests the protein may function to regulate the synapse and that LINCL may be a result of
123 synapse failure. We further examined the localization of Cln7 using a CRIPSR-generated
124 Venus-YFP-Cln7 knock-in and higher-resolution Airyscan 3D confocal imaging. We find that
125 Cln7 is restricted to a region overlapping with the basal sub-synaptic reticulum (SSR) (Fig. 1c-
126 f). The SSR is a convoluted membranous structure membrane in the post synaptic cell that
127 surrounds the pre-synaptic membrane swellings (the boutons) and contains the post-
128 synaptic glutamate receptors. Electron microscopy studies have revealed the SSR fully
129 surrounds the pre-synaptic bouton and anti-Discs large staining (DLG, the *Drosophila*
130 homologue of PSD-95), which marks the SSR, shows the same distribution (Fig. 1e and f).
131 Interestingly, the Cln7 protein appears to be associated with vesicles or the SSR membrane
132 network only on the basal side; Cln7 is not present surrounding the upper surface of the
133 bouton (Fig. 1c-f). Since retrograde signaling from the post synaptic cell is known to
134 influence synapse structure[9] we investigated the consequence of a loss of *Cln7* function.

135

136 *Cln7 is required for normal development of the NMJ*

137 We generated two loss-of-function alleles of *Cln7* by imprecise excision of the P-
138 element NP0345 inserted in the 5' UTR upstream of the start codon. Two alleles were
139 generated: exons 1-5 were excised in the $Cln7^{84D}$ allele, with some P-element sequence
140 remaining and exons 1 and 2 and part of exon 3 were excised in $Cln7^{36H}$. Both mutant alleles
141 are viable and fertile when homozygous and show no developmental delay. The peripheral
142 NMJs in late stage *Drosophila* larvae are simple, with 2-4 individual motoneurons contacting
143 each muscle cell. The type I motoneurons that innervate the muscle can be further
144 subdivided into two classes called type Ib and type Is classified according to the size of the

145 presynaptic boutons (Fig. 2a). We find that in *Cln7*$^{-/-}$ animals the NMJ is reduced in size. At
146 muscle 4 we see a significant reduction of the type Ib motoneuron terminals in the *Cln7*
147 mutant larvae when compared to isogenic control larvae (Fig. 2a). We used a non-subjective
148 method of measuring terminal volume from 3D-rendered confocal images to confirm the
149 type Ib terminals were significantly smaller than controls while the type Is terminals appear
150 unaffected (Fig. 2b). As a further measure of synapse size, we counted the number of active
151 zones at the NMJ. Active zones are visualized with an antibody to Bruchpilot (ELKS), an
152 active zone component[22]. Bruchpilot positive puncta were counted at muscle 4 and this
153 confirmed that the number of active zones within Ib boutons is reduced in *Cln7*$^{-/-}$ animals
154 concomitant with the reduction in volume but is unchanged in type Is junctions (Fig. 2c).
155 Both alleles of Cln7 had an identical phenotype as does the trans-heterozygous
156 combination. Both alleles were also haploinsufficient, suggesting some processes important
157 for NMJ development are critically dependent on the levels of the Cln7 protein: potentially
158 the stoichiometry of a membrane complex. These results reveal a requirement for Cln7 for
159 normal development of the NMJ.
160 To investigate whether Cln7 is required in the post synaptic cell we used RNAi to
161 reduce *Cln7* expression in various cell types at the synapse. Standard GAL4 drivers were
162 used to express dsRNA specifically targeted at *Cln7* either pre-synaptically (Elav-Gal4), post-
163 synaptically in the muscle (Mef2-Gal4), in all glia (Repo-Gal4) and in only the perineurial glia
164 (PG-Gal4) that form the blood-brain-barrier, where *Cln7* is also highly expressed[21]. Only
165 knockdown of *Cln7* in the muscle replicated the under-development phenotype at the NMJ
166 (Fig. 2d), consistent with the expression of *Cln7*. We also performed the converse
167 experiment of re-expressing YFP-Cln7 in the *Cln7*$^{-/-}$ background, again with ubiquitous
168 expression (actin-Gal4) or expression restricted to neurons (Elav-Gal4), to muscle (Mef2-
169 Gal4), in both neurons and muscle together (Spin-Gal4) or to glia (Repo-Gal4). Muscle
170 expression with Mef2- or Spin-Gal4 was only capable of partial rescue of function which
171 failed to reach significance. Only ubiquitous expression fully rescued the phenotype (Fig. 2e)
172 indicating that some Cln7 function is required elsewhere in addition to the muscle.
173
174

175 *Loss of Cln7 leads to synapse dysfunction*
176
177 To examine the functional consequence of the abnormal development of the
178 synapse we characterized synaptic physiology and larval motility. An electrophysiological
179 analysis of the NMJ was carried out using intracellular recordings. We recorded the
180 spontaneous transmitter release at the larval NMJs for two minutes to calculate miniature
181 excitatory junction potential (mEJP) frequency and amplitude in 0.5, 0.75, 1.0 and 2.0 mM
182 extracellular Ca^{2+} concentration but there was no significant difference due to genotype in
183 either case (Fig. 3a). Taken together, we concluded there was likely to be little overt change
184 in spontaneous synaptic vesicle release or post-synaptic receptor density.
185 Nerve-evoked excitatory junction potentials (EJPs), were recorded at 1 Hz frequency
186 at 1 mM extracellular Ca^{2+} to evaluate synapse function. We found that EJPs at *Cln7*
187 neuromuscular junctions were similar to those produced by control animals (Fig. 3b). We
188 next applied continuous 5 Hz stimulation to the motor neurons to assess changes in the
189 ability to recruit from the reserve pool of neurotransmitter vesicles. In the control animals,
190 the evoked amplitudes followed a trend towards mild depression as vesicles in the reserve
191 pool become depleted. However, a much more accentuated decline of EJP amplitude was
192 observed in *Cln7* mutant animals under the same conditions (Fig. 3c). This suggests a
193 potential defect in the ability of *Cln7* neurons to activate vesicles from the reserve pool or a
194 defect in synaptic vesicle recycling.
195 The NMJs regulate body-wall muscle contraction. To identify if the
196 electrophysiological changes we detected led to a quantifiable change in locomotion, we
197 measured instantaneous speed of larval crawling. To address large variations in behavior
198 within a population of larvae, and to overcome the tendency of larvae to avoid open fields,
199 we used a custom 3D printed chamber to record the movement of multiple larvae
200 simultaneously in oval "racetracks" over periods of 5 min (see methods). *Cln7* mutant larvae
201 move significantly more slowly than isogenic control larvae (Fig. 3d).
202
203 *Autophagy and BMP signaling is unaffected in Cln7 animals*
204
205 Cln7 is required in post synaptic cells for normal development and function of the
206 NMJ we investigated potential pathways of action. Impairment of autophagy is known to
207 cause a reduction in synapse size[24], similar to that seen in the *Cln7* mutants. Furthermore, in

208 cultured cells Cln7 is associated predominantly with lysosomes[15], which are essential
209 mediators of autophagy and mutations affecting lysosomal function lead to a block in
210 autophagic flux. We examined accumulation of p62, a multiple domain protein that acts as a
211 receptor to activate autophagy. Under nutrient-rich conditions, p62 is usually degraded in
212 lysosomes but in starvation conditions autophagic flux is increased and some non-degraded
213 p62 accumulates in lysosomes (Fig. 4a; see w^{1118} control). Thus, p62 levels are often
214 monitored as one readout of autophagic flux. In *Cln7* larvae no p62 accumulates under
215 growth conditions. However, a small but not statistically significant amount of p62 did
216 accumulate under starvation conditions in the *Cln7* larvae, suggested a minor impairment in
217 autophagy or lysosomal function (Fig. 4a). This contrasted markedly with *atg18* mutants.
218 Here, p62 clearly accumulated during growth and did so very dramatically under starvation
219 conditions (Fig. 4a).
220 We also examined whether increasing autophagic flux could rescue the *Cln7*
221 phenotype by inhibiting the TOR complex activity using rapamycin or torin. TORC1 is a
222 central regulator of growth and autophagy and homeostasis in cells and TORC2 is required
223 for normal NMJ development[15,23]. Inhibition of TORC1 increases autophagic flux which, in
224 the *Drosophila* NMJ, leads to an overgrowth phenotype[24]. Previously, it was reported that
225 inhibiting TORC1 with rapamycin was unable to rescue the smaller NMJ phenotype seen in
226 *atg18* mutants, presumably because autophagy is severely compromised in these animals
227 and this cannot be circumvented[24]. We reasoned that rapamycin treatment would similarly
228 have no effect on the *Cln7* phenotype if it was due to defective autophagy. However, both
229 rapamycin treatment or treatment with the TORC1 and TORC2 inhibitor, torin, caused a very
230 robust increase in NMJ size in both control and *Cln7* larvae indicating that autophagic flux
231 can be increased (Fig. 4b). Taken together with the lack of p62 accumulation, this suggests
232 that loss of Cln7 does not lead to an overt block in autophagy.
233 Given enrichment of Cln7 at the PSD we proceeded to investigate whether Cln7
234 functions in the classical retrograde signaling mediated by the post-synaptic BMP ligand
235 Glass-bottomed boat (Gbb). Loss of the type I BMP receptor Saxophone (Sax) leads to a
236 reduced NMJ of a size almost identical to that in *Cln7* larvae (Fig. 4c). However, a
237 $sax^{4/5}$;$Cln7^{84D}$ double mutant combination was lethal before late larval stage suggesting an
238 additive effect and indicating that Cln7 and Sax operate in different pathways. Conversely,
239 mutations in *Dad*, which encodes an inhibitory SMAD, lead to NMJ synapse overgrowth and

240 a profusion of small, satellite boutons (Fig. 4c). A *Dad*^{J1e4};*Cln7*^{84D} double mutant combination
241 showed a small reduction in overgrowth resulting in an intermediate phenotype. This
242 suggests that phosphorylation of Mad in response to a Gbb signal is intact in the *Cln7*
243 mutant larvae. To further confirm this, we stained the CNS of wild-type and *Cln7* larvae with
244 anti-pMad. The nuclei of motor neurons clearly showed pMad present at the synapse in
245 both genotypes (Fig. 4d) indicating that BMP signaling is unaffected in the absence of Cln7.
246
247 *Dysregulated TORC signaling in Cln7 mutants*
248 During our study, we noticed that the *Cln7* flies are considerably larger than their
249 isogenic control lines (Fig. 5a). *Cln7* flies are not only heavier than controls, their body parts
250 are also larger. We measured wing blade area from detached wings and identified a
251 significant increase in *Cln7* animals *vs.* controls (Fig. 5b). Increased wing size could be due to
252 additional cell divisions or larger cells. Additional divisions would suggest dysregulation of
253 cell cycle control, but larger cells could indicate a potential hyper-activation of TORC. We
254 measured the average area of cells within the wing and found a significant increase in cell
255 size in flies lacking Cln7 (Fig. 5b). Hyper-activation of TORC may also lead to excessive
256 storage of lipids[25]. We measured triacylgylcerides, the principal lipid stored in *Drosophila*
257 and identified that Cln7 flies have more than 2-fold greater lipid storage than control flies
258 (Fig. 5c).
259 Since TORC2 complex activity is necessary to restrict cell growth and loss of the
260 TORC2-specific component, Rictor, leads to a large expansion of the NMJ[23], we wondered
261 whether Cln7 may function in a pathway regulated by TORC2. We generated a
262 *rictor*$^{\Delta 42}$;*Cln7*^{84D} double mutant and found that these animals have a significantly reduced
263 mass identical to that of *rictor*$^{\Delta 42}$ single mutants (Fig. 5d). Similarly, the *rictor*$^{\Delta 42}$;*Cln7*^{84D}
264 double mutant show an expanded NMJ indistinguishable in size from the *rictor*$^{\Delta 42}$ single
265 mutant (Fig. 5e). This places *Cln7* genetically upstream of TORC2 but, as with autophagic
266 flux, TORC2 activity appears to be function principally in the neuron downstream of Tsc2[23].
267 Given the restriction of Cln7 to the post-synaptic side, it is not likely to be directly acting on
268 TORC2 in the neuron but could feasibly regulate TORC2 indirectly via a retrograde signal.
269 We looked for further supporting evidence that TORC is dysregulated by loss of Cln7.
270 We stained NMJs with an antibody to phosphorylated pS6, which is a marker of TORC1
271 activity. Phosphorylated S6 was seen clearly to localise at active zones in the pre-synaptic

272 boutons, suggesting localised activation of TORC1 at these release sites (Fig. 5f). This pattern
273 was retained in the Cln7 mutant NMJ (Fig. 5g), consistent with the restriction of Cln7 to the
274 post-synaptic side and acting through TORC2 rather than TORC1 in neural development.
275 Interestingly, some pS6 staining was seen in a vesicular pattern throughout the muscle and
276 this was reduced in the Cln7 mutant (Fig. 5g).
277 Next, we looked for more direct biochemical support that Cln7 regulates TORC
278 activity. Rheb is a small GTPase located primarily in the lysosomal membrane and
279 potentially co-located with Cln7, so we investigated whether Cln7 might be in a protein
280 complex with Rheb. We expressed tagged forms of Cln7 and Rheb in *Drosophila* S2 cells and
281 were able to co-immunoprecipitate the two proteins (Fig. 5g).
282 Finally, we switched to mammalian cells to confirm that the involvement of Cln7 in
283 the regulation of TORC signalling is conserved. We starved control and *Cln7*$^{-/-}$ mouse
284 embryonic fibroblasts cells to reduce basal TORC activity and then returned insulin, amino
285 acids or glucose to the cells. In each case, a robust of activation of TORC1 leading to
286 activation phosphorylation of p70 S6 kinase (Fig. 5h). In contrast, TORC1 fails to be activated
287 after starvation in *Cln7*$^{-/-}$ cells, consistent with a previous report[20].
288
289 **Discussion**
290 We have uncovered a role for Cln7 in the regulation of synapse growth and
291 development through a retrograde signaling process from the post-synaptic cell. TORC
292 signaling is dysregulated by loss of Cln7, potentially though disruption of a Cln7 and Rheb-
293 containing membrane complex. Interestingly, Cln7 mutant flies show classic indications of
294 excessive TORC1 activity leading to larger cell size, increased mass and excessive lipid
295 storage yet blocking TORC2 activity reverses these phenotypes. TORC1 activity fails to
296 reactivate in *Cln7*$^{-/-}$ cells after starvation indicating Cln7 function is conserved across species.
297 TOR has a conserved postsynaptic role to influence retrograde regulation of synaptic
298 activity at central and peripheral synapses in both *Drosophila* and vertebrates[13,26]. Several
299 activating mutations upstream of mTORC1, including loss of PTEN or Tsc1/2, result in
300 overgrowth of neurons and increase in density of dendritic spines in the mammalian CNS[27].
301 Less is understood about the role of the mTORC2 complex in the CNS although deletion of
302 the TORC2-specific component, Rictor, in all neurons or specifically in Purkinje cells causes

303 deficits in neural growth and development, including morphological effects with
304 consequential early-onset motor deficits[28,29].
305 Studies in *Drosophila* have revealed that TOR signaling is required for normal
306 synapse function and regulates multiple pathways controlling diverse mechanisms in both
307 the pre- and post-synapse partners. Reduced TORC1 activity in the pre-synapse can limit JNK
308 activity required for presynaptic membrane growth[11] where TORC2 also stimulates Akt
309 activity necessary to limit presynaptic membrane addition[23]. The TOR target Akt is also
310 required in the postsynaptic cell for the growth and assembly of the sub-synaptic reticulum
311 and targeting of glutamate receptor subunits to the postsynaptic cell surface necessary for
312 synapse expansion[30]. Additionally, TOR-mediated regulation of S6 kinase and presence of
313 the translation initiation factor eIF4E level is needed in the postsynaptic cell to produce an
314 unknown retrograde signal that regulates pre-synaptic neurotransmitter release[13]. It
315 remains to be discovered how Cln7 precisely influences TOR signaling to mediate
316 appropriate synapse growth and homeostasis.
317 The conserved role for TORC in regulating synaptic development has implications for
318 human CLN7 disease (also known as late-infantile neuronal ceroid lipofuscinosis). Our data
319 suggest dysregulated mTORC activity leading to developmental synaptic pathology may
320 underpin the disease. It is also significant that Cln7 protein was recently found to co-localise
321 with the post-synaptic marker, PSD-95, in the outer plexiform layer of the murine retina[31];
322 loss of visual acuity is an early symptom in CLN7 disease in humans.
323

324 **Methods**

325 ***Drosophila* lines.**
326 *Drosophila* lines were obtained from the Bloomington Stock Center at Indiana University except for
327 an isogenic w^{1118} control strain from the Vienna *Drosophila* Resource Center; PG-Gal4 (*NP6293) from*
328 *the Kyoto DGRC Stock Center*; Spin-Gal4 and Dad^{j1e4} from Dr. Sean Sweeney (University of York, UK);
329 and $rictor^{\Delta 42}$ from Dr. Joseph Bateman (King's College London). Gal4 lines used with stock numbers
330 as of March 2018 were as follows: actin (BL3954); $Elav^{c155}$ (BL458); Mef2 (BL27930); vGlut (BL26160);
331 Repo (BL7415); PG (Kyoto: 105188). The Cln7 RNAi line used was yv;TRiP.HMC03819 (BL55664). To
332 generate UAS-Venus-Cln7, the full-length Cln7 ORF was amplified by proofreading PCR using clone
333 GH22722 as a template and cloned into pENTR (Thermo). After sequence verification it was

334 recombined into the pTVW destination vector obtained from the *Drosophila* Genetics Resource
335 Center, University of Indiana and transformants generated by BestGene Inc.
336
337 **Generation of Cln7 mutants.**
338 The P-element NP0345 inserted in the 5'UTR of the *Cln7* locus (CG8596) was excised by mating with
339 to the Δ2-3 transposase line. Two independent alleles, 36H and 84D, were backcrossed over 6
340 generations to the isogenic w^{1118} control.
341
342 **Visualization of the larval NMJ**
343 The pre-synaptic membrane was visulaised with Alexa-594 goat anti-HRP (1;1000; Jackson Immuno)
344 except for volume measurements from confocal z-sections when a membrane-localized GFP was
345 used (OK371-Gal4, UAS-CD8::GFP) with rabbit anti-GFP (AbCam, 1:1000). To ensure constant culture
346 density and conditions between samples, cohorts of 100 1st instar larvae were picked from the agar
347 plates and transferred to vials of freshly made food and incubated for 3-4 days until wandering 3rd
348 instar stage. Larval flatmounts were immunostained using standard procedures, mounted in Prolong
349 Gold (Thermo) and visualized on a Zeiss LSM510 Meta, LSM780 or LSM880 Airsycan confocal
350 microscopes using using 40X N.A. 1.4 oil immersion, 40X N.A. 1.2 water immersion or 100x N.A. 1.42
351 oil immersion PlanApo lenses, respectively. 3D Renders were processed in Volocity (Perkin Elmer).
352 Active zones were stained with mouse anti-Bruchpilot (clone NC82, 1:25; Developmental Studies
353 Hybridoma Bank) and post-synaptic densities with anti-Dlg (clone 4F3, 1:20; DSHB). Rabbit anti-
354 pMAD (1:500) was a gift of Prof. Carl-Henrik Heldin (Ludwig Institute for Cancer Research, Uppsala).
355 YFP-Cln7 was visualized with rabbit anti-GFP (1:5000; AbCam ab290). Rabbit anti-pS6 (1:400) was a
356 kind gift of Dr. Jongkyeong Chung, Seoul National University[32].
357
358 **Quantification of NMJ size**
359 Volumes were acquired with an optical slice width of 1.0 µM and steps of 0.5 µM using a 40x N.A. 1.4
360 PlanApo objective and zoom = 2.0. Volocity was used to render the volumes then to measure the
361 volume of the pre-synaptic membrane and to count active zones. Boutons were counted manually
362 for the type Ib junction on muscle 4 of segments A3-A5. In each case a transmitted light image of the
363 corresponding muscle was obtained at 10x and the muscle surface area calculated by outlining in
364 ImageJ. Bouton number was then normalized to the muscle surface area.
365
366 **Quantification of larval movement**
367 Wandering 3rd instar stage larvae were transferred to a custom 3D-printed chamber comprising 12

368 oval troughs each 3 mm deep and with a track length of 75 mm. Each trough was lined with a thin
369 coating of 3% w/v agar. The chamber was lit from below by a LED light table and filmed from above
370 with a Basler GigE camera. Cohorts of 12 larvae crawling were filmed for 5 min each and their
371 position tracked at 2.5 fps using Ethovision software (Noldus).
372
373 **Electrophysiology**
374 Wandering 3rd instar larvae were dissected in HL3.1 supplemented with Ca^{2+} concentration at 0.5,
375 0.75, 1.0 or 2.0 mM depending on the paradigm[33]. Recordings were made from muscle 4 of
376 segments A3-A5 using standard protocols[34]. Baseline synaptic transmission was characterized by
377 recording mEJPs for 2 min and 16 EJPs stimulated at 1 Hz. For high frequency stimulation, 16 EPSPs
378 at 1 Hz were recorded followed by 5 Hz stimulation for 5 min. In all experiments a minimum of 8
379 larvae were used with maximum of 2 recordings per larva. In each case the starting resting potential
380 of the muscle was -60 to -75 mV and resistance of 5-10 mΩ. Analysis of electrophysiological
381 recordings was performed in Clampfit 10.0 (Molecular Devices) and data exported for further
382 analysis in Prism 7.0 (Graphpad).
383
384 ***Drosophila* starvation assay**
385 First instar larvae of control w^{1118}, $Cln7^{84D}$ and Atg18a$^{KG03090/}$Df(3L)Exel6112 were transferred in
386 cohorts of 20 from grape juice agar plates to standard food vials smeared with fresh yeast paste and
387 allowed to develop for a further 24 h at 25 °C. Larvae were then removed from the food and protein
388 samples prepared for each genotype. The remaining 10 larvae for each genotype were starved of
389 amino acids for 4 h at 25 °C. Lysates of total protein were prepared by manually crushing the larvae
390 with a mini-pestle directly into 200 µl Laemmli buffer containing 8 mM DTT and protease inhibitors.
391
392 **Cell transfection and immunoprecipitation.**
393 To generate expression plasmids, the Cln7 pENTR clone was recombined into pAMW. The full-length
394 Rheb ORF was amplified from clone GH10361 and cloned in to pENTR. After sequence verification it
395 was recombined in pAFW. Tagged proteins were immunoprecipitated with Myc-Trap_MA beads
396 (ChromoTek) or anti-FLAG M2 Affinity gel (Sigma) overnight at 4°C.
397
398 **Serum withdrawal experiments**
399 Mouse embryonic fibroblasts were seeded at 20% confluence then incubated in DMEM + 10 % FCS
400 (both Thermo) for 24 h. Cells were then washed once in EBSS (Thermo) and then starved for 18 h in
401 1 ml of EBSS. For re-feeding, the EBBS was replaced with complete medium (EBSS plus 10% dialysed

402 FBS (USB Biologicals), 1x amino acid mix (Thermo), 5.5 mM D-glucose, 4 µg/mL insulin, pH 7.95) or
403 partial recovery medium lacking either the amino acids, the glucose or the insulin. For the non-
404 starved control, basal DMEM + 10% FCS was used. Cells were lysed directly in the culture dishes after
405 1 h in 1X RIPA buffer (New England Biolabs) then clarified by centrifugation at 15,000 x g for 10 min
406 at 4°C. The protein concentration of the supernatants was determined by Pierce 660 nm protein
407 assay before SDS-PAGE and Western blotting.
408
409 **Western blotting**
410 Protein were separated by standard SDS-PAGE and transferred to PVDF membranes by wet transfer.
411 Primary antibodies were: mouse anti-Flag M2 (1:5000; Sigma); goat anti-myc (1:1000; AbCam
412 ab9132); rabbit anti-Ref(2)P (*Drosophila* homologue of p62, 1:500; a gift of Dr. Gabor Juhasz, Eötvös
413 Loránd University, Budapest); rabbit anti-p70 S6K pThr389 (1:500; Cell Signaling Technologies) and
414 mouse anti-actin (clone JLA-20, 1:500; DSHB). Secondary antibodies were HRP-conjugated goat anti-
415 mouse or anti-rabbit IgG (both 1:4000, Cell Signaling Technologies). Detection of HRP was with
416 SuperSignal West femto ECL reagent (Pierce) in conjunction with a Vilber Fusion FX system. p62
417 levels were normalized to actin from 16-bit images using ImageJ.
418
419 **Statistical analysis**
420 All statistical tests were performed within Prism 7 (GraphPad). Normality of datasets was
421 determined using a D'Agostino-Pearson test and datasets not conforming to Gaussian distributions
422 were transformed with logarithmic or reciprocal transformations. Non-parametric tests were used
423 where distributions remained non-Gaussian after transformation. Samples sizes and tests used are
424 described in the figure legends. Significance in all cases was set at $p<0.05$.
425

426 ## Acknowledgements

427 The authors are very grateful to Dr. Stephan Storch for sharing the *Cln7*$^{tm1d/tm1d}$ mouse embryonic
428 fibroblasts ahead of publication; to Drs. Sean Sweeney and Joe Bateman for sending *Drosophila*
429 lines; and to Dr. Gabor Juhasz, Prof. Carl-Henrik Heldin and Dr. Jongkyeong Chung for the anti-
430 Ref(2)P, anti-pMad and anti-pS6 antibodies, respectively. Research was funded by The Wellcome
431 Trust grant number 082004 to GT and by a UK Biotechnology and Biological Sciences Research
432 Council New Investigator award BB/N008472/1 to RIT. BAS was supported by a Natural Sciences and
433 Engineering Research Council of Canada grant number 250078. MO'H was supported by a King's
434 College, London Quota BBSRC PhD studentship and a KCL Peter Baker Travelling Fellowship. AM and
435 KJC were supported by University of Birmingham College of Medical and Dental Sciences PhD

studentship awards. The authors declare no competing financial interests. All data will be made available upon reasonable request to the corresponding authors.

439 **References**

440

441 1 Davis, G. W. Homeostatic control of neural activity: from phenomenology to
442 molecular design. *Annu Rev Neurosci* **29**, 307-323,
443 doi:10.1146/annurev.neuro.28.061604.135751 (2006).
444 2 Turrigiano, G. G. The self-tuning neuron: synaptic scaling of excitatory synapses. *Cell*
445 **135**, 422-435, doi:10.1016/j.cell.2008.10.008 (2008).
446 3 Marques, G. Morphogens and synaptogenesis in Drosophila. *J Neurobiol* **64**, 417-434,
447 doi:10.1002/neu.20165 (2005).
448 4 Deshpande, M. & Rodal, A. A. The Crossroads of Synaptic Growth Signaling,
449 Membrane Traffic and Neurological Disease: Insights from Drosophila. *Traffic* **17**, 87-101,
450 doi:10.1111/tra.12345 (2016).
451 5 Bayat, V., Jaiswal, M. & Bellen, H. J. The BMP signaling pathway at the Drosophila
452 neuromuscular junction and its links to neurodegenerative diseases. *Curr Opin Neurobiol* **21**,
453 182-188, doi:S0959-4388(10)00134-0 [pii]10.1016/j.conb.2010.08.014 (2011).
454 6 Davis, G. W. & Goodman, C. S. Synapse-specific control of synaptic efficacy at the
455 terminals of a single neuron. *Nature* **392**, 82-86 (1998).
456 7 Collins, C. A. & DiAntonio, A. Synaptic development: insights from Drosophila.
457 *Current opinion in neurobiology* **17**, 35-42, doi:10.1016/j.conb.2007.01.001 (2007).
458 8 Frank, C. A. *et al.* New approaches for studying synaptic development, function, and
459 plasticity using Drosophila as a model system. *J Neurosci* **33**, 17560-17568,
460 doi:10.1523/JNEUROSCI.3261-13.2013 (2013).
461 9 Harris, K. P. & Littleton, J. T. Transmission, Development, and Plasticity of Synapses.
462 *Genetics* **201**, 345-375, doi:10.1534/genetics.115.176529 (2015).
463 10 Collins, C. A., Wairkar, Y. P., Johnson, S. L. & DiAntonio, A. Highwire restrains synaptic
464 growth by attenuating a MAP kinase signal. *Neuron* **51**, 57-69, doi:S0896-6273(06)00439-9
465 [pii]
466 10.1016/j.neuron.2006.05.026 (2006).
467 11 Wong, C. O. *et al.* Diminished MTORC1-Dependent JNK Activation Underlies the
468 Neurodevelopmental Defects Associated with Lysosomal Dysfunction. *Cell reports* **12**, 2009-
469 2020, doi:10.1016/j.celrep.2015.08.047 (2015).
470 12 Milton, V. J. & Sweeney, S. T. Oxidative stress in synapse development and function.
471 *Dev Neurobiol* **72**, 100-110, doi:10.1002/dneu.20957 (2012).
472 13 Penney, J. *et al.* TOR is required for the retrograde regulation of synaptic
473 homeostasis at the Drosophila neuromuscular junction. *Neuron* **74**, 166-178,
474 doi:10.1016/j.neuron.2012.01.030 (2012).
475 14 Charng, W. L., Yamamoto, S. & Bellen, H. J. Shared mechanisms between Drosophila
476 peripheral nervous system development and human neurodegenerative diseases. *Curr Opin*
477 *Neurobiol* **27**, 158-164, doi:10.1016/j.conb.2014.03.001 (2014).
478 15 Sharifi, A. *et al.* Expression and lysosomal targeting of CLN7, a major facilitator
479 superfamily transporter associated with variant late-infantile neuronal ceroid lipofuscinosis.
480 *Hum Mol Genet*, doi:ddq381 [pii]
481 10.1093/hmg/ddq381 (2010).
482 16 Kousi, M. *et al.* Mutations in CLN7/MFSD8 are a common cause of variant late-
483 infantile neuronal ceroid lipofuscinosis. *Brain* **132**, 810-819, doi:awn366 [pii]
484 10.1093/brain/awn366 (2009).

485 17 Aby, E. *et al.* Mutations in palmitoyl-protein thioesterase 1 alter exocytosis and
486 endocytosis at synapses in Drosophila larvae. *Fly* **7**, 267-279, doi:10.4161/fly.26630 (2013).
487 18 Kielar, C. *et al.* Molecular correlates of axonal and synaptic pathology in mouse
488 models of Batten disease. *Human molecular genetics* **18**, 4066-4080,
489 doi:10.1093/hmg/ddp355 (2009).
490 19 Grunewald, B. *et al.* Defective synaptic transmission causes disease signs in a mouse
491 model of juvenile neuronal ceroid lipofuscinosis. *Elife* **6**, doi:10.7554/eLife.28685 (2017).
492 20 Danyukova, T. *et al.* Loss of CLN7 results in depletion of soluble lysosomal proteins
493 and impaired mTOR reactivation. *Hum Mol Genet* **27**, 1711-1722, doi:10.1093/hmg/ddy076
494 (2018).
495 21 Mohammed, A., O'Hare, M. B., Warley, A., Tear, G. & Tuxworth, R. I. in vivo
496 localization of the neuronal ceroid lipofuscinosis proteins, CLN3 and CLN7, at endogenous
497 expression levels. *Neurobiology of disease* **103**, 123-132, doi:10.1016/j.nbd.2017.03.015
498 (2017).
499 22 Wagh, D. A. *et al.* Bruchpilot, a protein with homology to ELKS/CAST, is required for
500 structural integrity and function of synaptic active zones in Drosophila. *Neuron* **49**, 833-844,
501 doi:10.1016/j.neuron.2006.02.008 (2006).
502 23 Natarajan, R., Trivedi-Vyas, D. & Wairkar, Y. P. Tuberous sclerosis complex regulates
503 Drosophila neuromuscular junction growth via the TORC2/Akt pathway. *Human molecular*
504 *genetics* **22**, 2010-2023, doi:10.1093/hmg/ddt053 (2013).
505 24 Shen, W. & Ganetzky, B. Autophagy promotes synapse development in Drosophila. *J*
506 *Cell Biol* **187**, 71-79, doi:10.1083/jcb.200907109 (2009).
507 25 Caron, A., Richard, D. & Laplante, M. The Roles of mTOR Complexes in Lipid
508 Metabolism. *Annu Rev Nutr* **35**, 321-348, doi:10.1146/annurev-nutr-071714-034355 (2015).
509 26 Henry, F. E. *et al.* A Unique Homeostatic Signaling Pathway Links Synaptic Inactivity
510 to Postsynaptic mTORC1. *The Journal of neuroscience : the official journal of the Society for*
511 *Neuroscience* **38**, 2207-2225, doi:10.1523/JNEUROSCI.1843-17.2017 (2018).
512 27 Tavazoie, S. F., Alvarez, V. A., Ridenour, D. A., Kwiatkowski, D. J. & Sabatini, B. L.
513 Regulation of neuronal morphology and function by the tumor suppressors Tsc1 and Tsc2.
514 *Nat Neurosci* **8**, 1727-1734, doi:10.1038/nn1566 (2005).
515 28 Angliker, N., Burri, M., Zaichuk, M., Fritschy, J. M. & Ruegg, M. A. mTORC1 and
516 mTORC2 have largely distinct functions in Purkinje cells. *Eur J Neurosci* **42**, 2595-2612,
517 doi:10.1111/ejn.13051 (2015).
518 29 Thomanetz, V. *et al.* Ablation of the mTORC2 component rictor in brain or Purkinje
519 cells affects size and neuron morphology. *J Cell Biol* **201**, 293-308,
520 doi:10.1083/jcb.201205030 (2013).
521 30 Lee, H. G., Zhao, N., Campion, B. K., Nguyen, M. M. & Selleck, S. B. Akt regulates
522 glutamate receptor trafficking and postsynaptic membrane elaboration at the Drosophila
523 neuromuscular junction. *Dev Neurobiol* **73**, 723-743, doi:10.1002/dneu.22086 (2013).
524 31 Khan, K. N. *et al.* Specific Alleles of CLN7/MFSD8, a Protein That Localizes to
525 Photoreceptor Synaptic Terminals, Cause a Spectrum of Nonsyndromic Retinal Dystrophy.
526 *Investigative ophthalmology & visual science* **58**, 2906-2914, doi:10.1167/iovs.16-20608
527 (2017).
528 32 Kim, W., Jang, Y. G., Yang, J. & Chung, J. Spatial Activation of TORC1 Is Regulated by
529 Hedgehog and E2F1 Signaling in the Drosophila Eye. *Dev Cell* **42**, 363-375 e364,
530 doi:10.1016/j.devcel.2017.07.020 (2017).

531 33 Stewart, B. A., Atwood, H. L., Renger, J. J., Wang, J. & Wu, C. F. Improved stability of
532 Drosophila larval neuromuscular preparations in haemolymph-like physiological solutions. *J*
533 *Comp Physiol A* **175**, 179-191 (1994).
534 34 Zhang, B. & Stewart, B. Electrophysiological recording from Drosophila larval body-
535 wall muscles. *Cold Spring Harbor protocols* **2010**, pdb prot5487, doi:10.1101/pdb.prot5487
536 (2010).
537

538

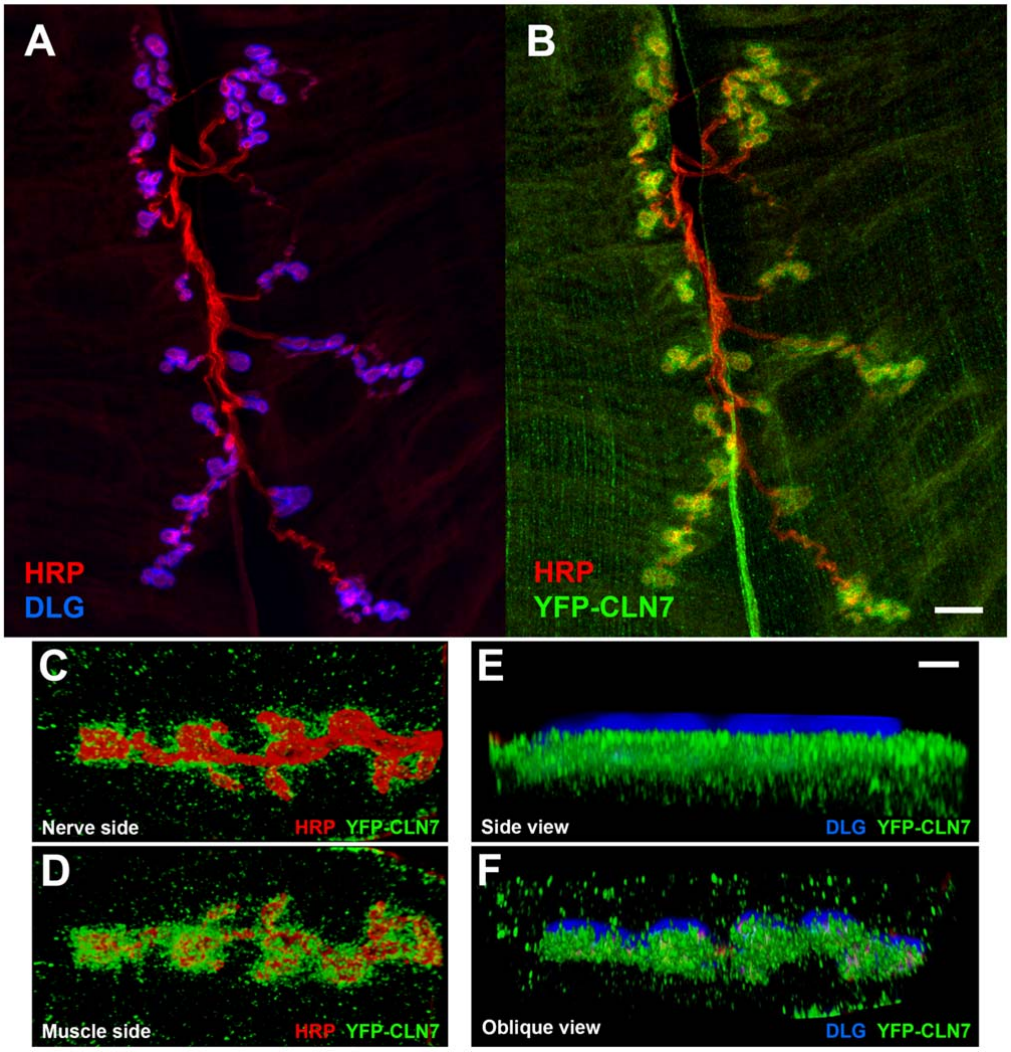

Figure 1. Cln7 localizes to the basal sub-synaptic reticulum at the neuromuscular junction. A-B): Immunofluorescence staining of the NMJ at muscle 6/7 stained with anti-HRP to visualize the neuronal membrane (red in A and B), anti-DLG for the sub-synaptic reticulum (SSR; blue in A) and anti-GFP to show YFP-Cln7 localization (green in B). YFP-Cln7 is concentrates at the SSR. Scale bar = 10 µm. C-E): Higher Airyscan resolution imaging of boutons at NMJ3, rendered into 3D and rotated using Volocity. Note the four panels are from the same acquired image and show anti-GFP (green) with either anti-HRP (red; C&D) or anti-DLG (blue; E&F). YFP-Cln7 localizes in a vesicular pattern around the boutons but is restricted to the basal part of SSR (view from muscle side, D). GFP staining is largely absent from the SSR above the boutons (view from side, E; GFP and DLG overlap below the boutons only).

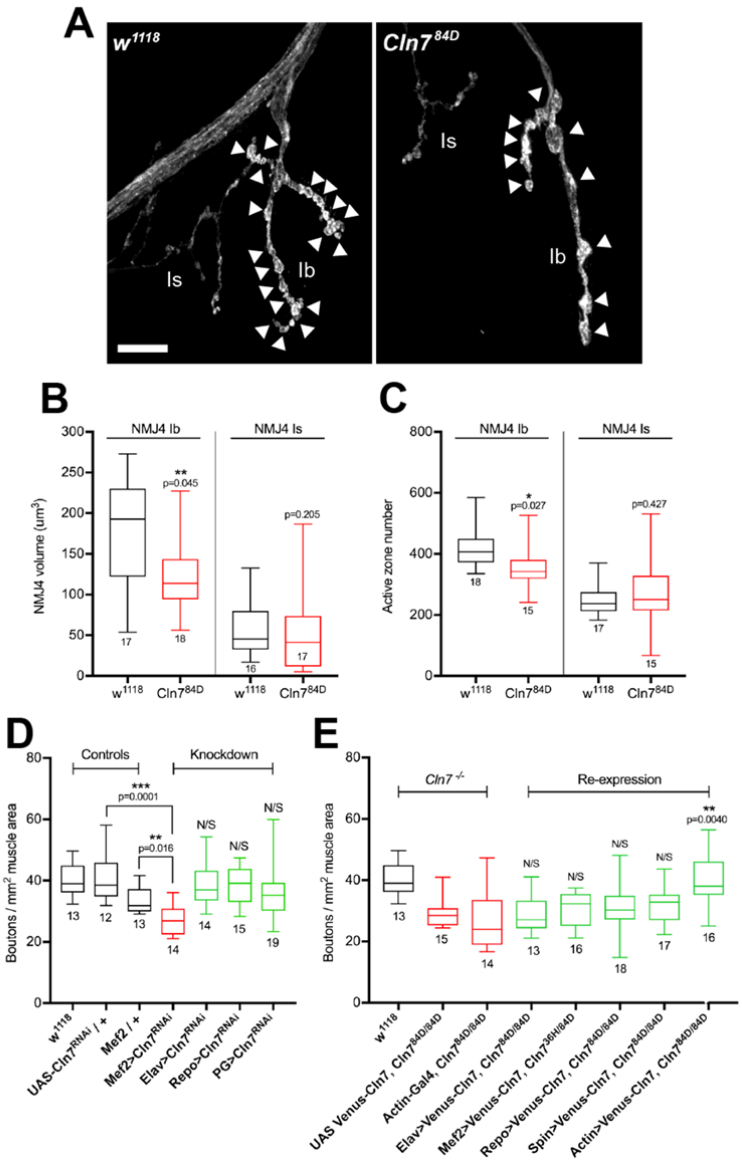

Figure 2. Loss of Cln7 leads to neurodevelopmental defects.

A). Anti-HRP staining of the late larval NMJ of *w*^{1118} control and *Cln7*^{84D} flies to visualize the neuronal membrane. Swellings of the pre-synaptic membrane (boutons) are indicated with arrowheads. There are fewer boutons in *Cln7*^{84D} larvae but these are occasionally swollen. Scale bar = 10 µm. B). The volume of type Ib junction is reduced in *Cln7*^{84D} flies but the type Is junction is unchanged. C). Active zones number is reduced in *Cln7*^{84D} type Ib but not in type Is junctions. (B&C; 2-tailed t-tests, n is indicated). D). The number of boutons can be used as a proxy for junction size. Type Ib junctions are smaller when *Cln7* expression is knocked down post-synaptically in muscle (Mef2-gal4) but not with pre-synaptic (Elav), pan-

563 glial (Repo) or perineurial glial knockdown (PG). E). Normal NMJ development is restored
564 only when Cln7 is re-expressed ubiquitously (actin-Gal4) in the mutant background. (D&E:
565 ANOVA with Dunnett's post-hoc comparisons, n is indicated).
566

567

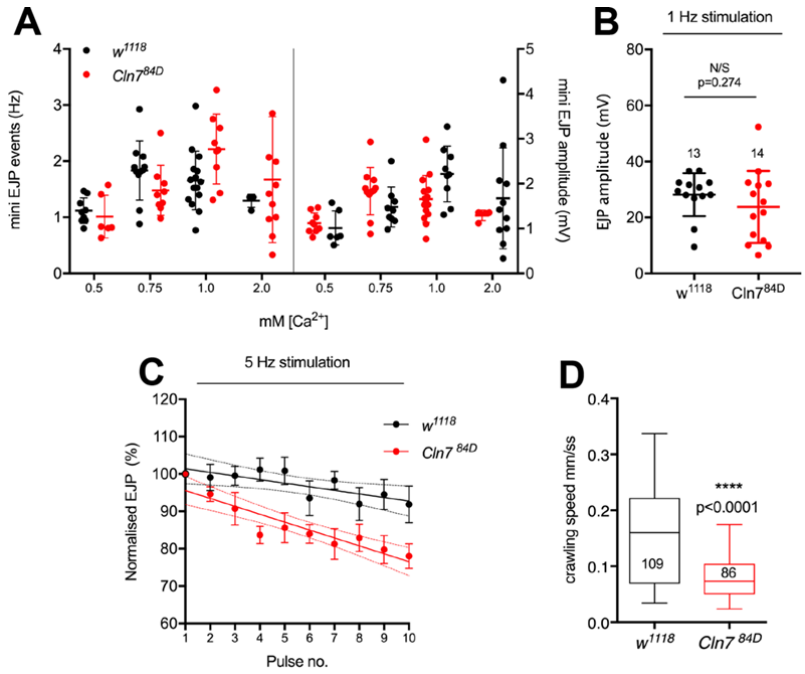

568

569

570 **Figure 3. Altered neural function in *Cln7* mutant flies**

571 A-C): Electrophysiological recordings from muscle 4 in *w1118* control and *Cln7*^{84D} larvae. A.
572 The frequency (A) and amplitude (B) of miniature excitatory junction potentials (mEJP) are
573 not significantly changed in *Cln7* larvae. mEJP frequency (left) was calculated over 120 s for
574 each larva and amplitude (right) from 201-835 events using four different concentrations of
575 extraceullular Ca^{2+}. Mean is indicated by a solid bar; error bars indicate SD. 2-way ANVOA
576 with Sidak's multiple comparisons. F = 0.6086; DFn = 1; DFd = 66; p=0.4381 for both. B.
577 Excitatory junction potentials (EJPs) are unchanged in Cln7 larvae. The mean of 16 EJPs at 1
578 Hz was calculated from n=13 (*w*^{1118}) or 14 (*Cln7*^{84D}) in 1 mM Ca^{2+}. Mean is indicated by a
579 solid line; error bars show SD. p=0.274; Mann-Whitney. C). *Cln7* mutant synapses display an
580 increased rate of fatigue at 5 Hz stimulation. EJP amplitude at 5 Hz was normalised to the
581 mean amplitude at 1 Hz stimulation immediately beforehand. n=4 NMJs for *w*^{1118} and =6 for
582 *Cln7*^{84D}. Trend lines fitted by linear regression are shown with solid lines with 95%
583 confidence intervals indicated by dashes. R^2: *w*^{1118} = 0.149; *Cln7*^{84D} = 0.383. The slopes are
584 significantly different: F= 4.786; DFn = 1; DFd = 96; p=0.0311, t-test. D). Crawling speed is
585 reduced in *Cln7*^{84D} larvae. Mean speed of *w*^{1118} control (n=109) and *Cln7*^{84D} (n=86) larvae
586 was determined at 2.5 fps over 5 mins. **** p<0.0001; Mann-Whitney.

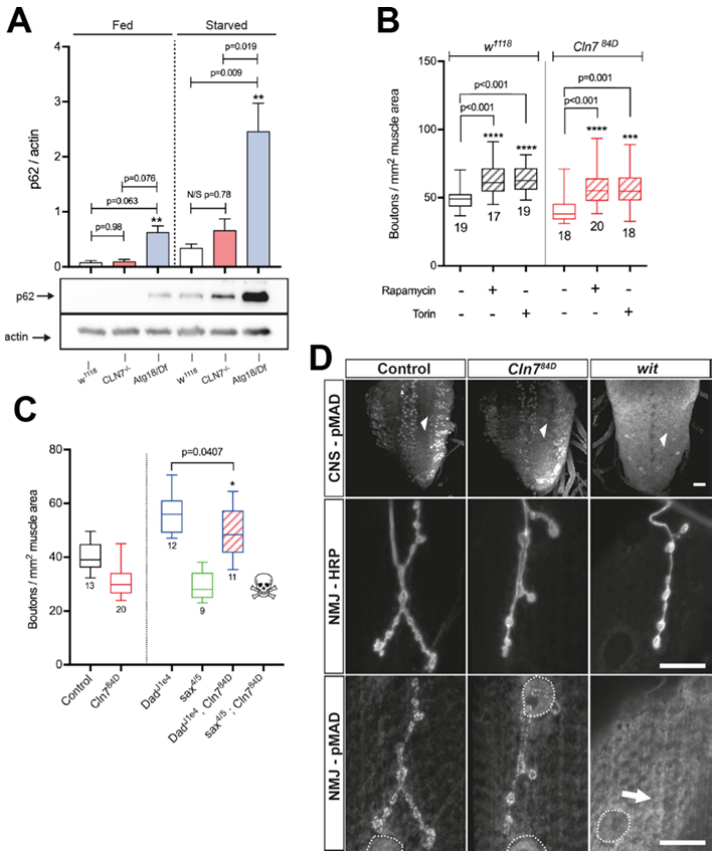

587

588

589 **Figure 4. Autophagy and retrograde BMP signaling are unaffected by loss of Cln7.**

590 A-B). The lysosomal substrate, p62, does not accumulate in control of *Cln7*^{84D} larvae when
591 feeding but does in *atg18* mutants. A. After 4 h starvation, p62 accumulates in control
592 animals. Accumulation is slightly but not significantly increased in *Cln7*^{84D} larvae. In contrast,
593 p62 accumulates to very high levels in starved *atg18* mutants. Bars show mean p62 band
594 intensity +/- SEM normalised to actin, n=3 for each. ** p<0.01, ANOVA. C). Inhibition of
595 TORC1 with Rapamycin or TORC1 and 2 by Torin drives NMJ overgrowth by increasing
596 autophagic flux. *Cln7* mutant larvae respond similarly to control *w*^{1118} larvae suggesting no
597 block in autophagy. *** p=0.01; **** p<0.001; ANOVA with Dunnett's post-hoc
598 comparisons, n is indicated. C). Mutations affecting retrograde signaling from the muscle
599 alter neural development. Mutations in the inhibitory SMAD, *Dad*, drive overgrowth of the
600 NMJ; mutations in the *saxophone* type I TGFβ receptor result in underdevelopment at a
601 similar level to *Cln7* mutants. A double *Dad;Cln7* mutant displays a small but significant
602 moderation of the *Dad* phenotype (2-tailed t-test: t=2.181, Df=21, p=0.0407). A *sax;Cln7*
603 double mutant is lethal early in development. Control *w*^{1118} and *Cln7*^{84D} data from Fig.2 are

604 included for comparison. D). Mad is phosphorylated after binding of the Gbb ligand to Tkv,
605 Sax and Wit receptors in the neuron. Characteristic pMad staining is clearly visible in
606 columns of motor neurons in the control and *Cln7*^{84D} CNS but is absent in a *wit* mutant CNS
607 (anti-pMad, top row, arrowheads). pMad staining in boutons is also present in boutons in
608 control and *Cln7*^{84D} NMJs but absent in a *wit* mutant (anti-pMad, bottom column; anti-HRP
609 marks the neuronal plasma membrane, middle column). Similarly, pMad is localised within
610 muscle nuclei but absent in *wit* mutants (dashed circles). Scale bar = 20 µM.
611

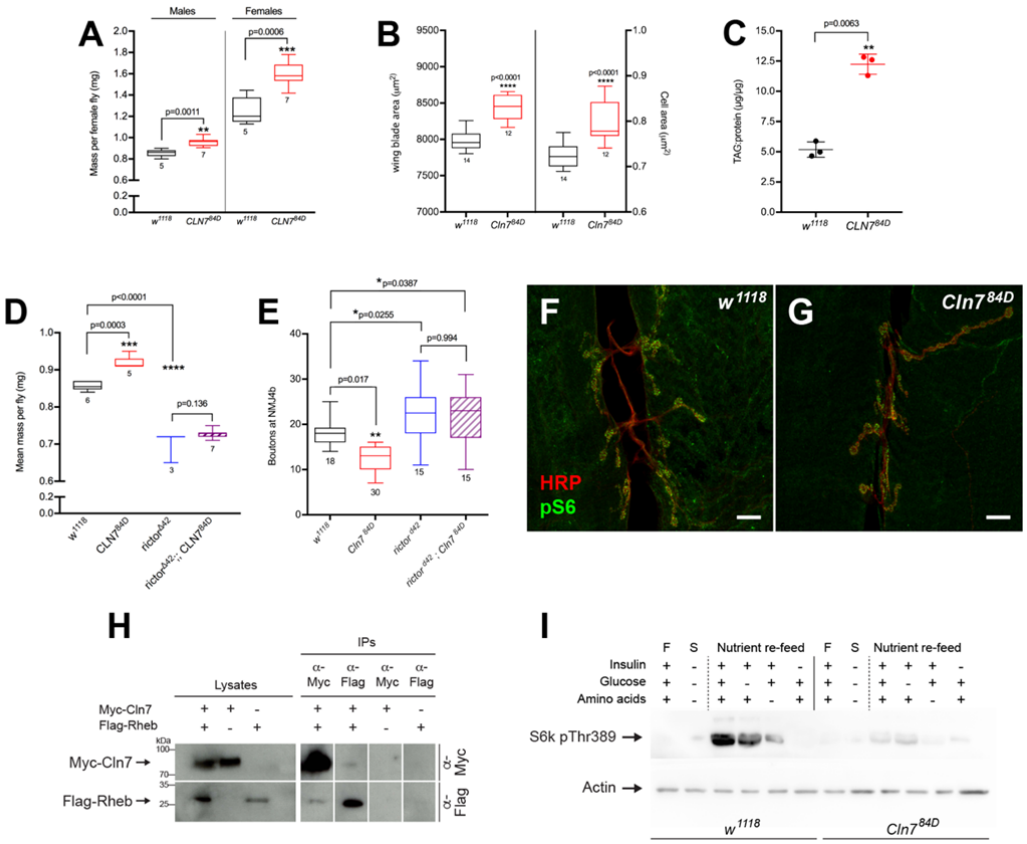

Figure 5. Loss of Cln7 leads to dysregulation of TORC

A). *Cln7*^{84D} flies are significantly larger than isogenic *w*^{1118} controls. The mean mass of adult flies is shown. B). *Cln7*^{84D} female flies have larger wings than *w*^{1118} controls due to increased cell size, C). *Cln7*^{84D} female flies higher levels of triacylgylceride (TAG) storage than *w*^{1118} controls. TAG concentration normalized to protein concentration is shown for n=3. (A-C: 2-tailed t-tests, n is indicated for A&B). D-E). Cln7 is genetically upstream of TORC2 signaling. D). Flies mutant for the TORC2 component, *rictor,* are smaller than controls and a *rictor;;Cln7* double mutant displays a *rictor* phenotype E). *rictor*$^{\Delta 42}$ larvae have overgrown type 1b junctions. A *rictor;;Cln7* double mutant also shows an overgrowth phenotype (D&E: ANOVA with Dunn's post-hoc comparisons, n is indicated). F). Immunofluorescence of NMJ6/7 stained for pre-synaptic membrane (anti-HRP, red) and TORC1 activity (anti-pS6, green). pRpS6 is phosphorylated by TORC1. Distinct foci of pS6 are present at the active zones in pre-synaptic boutons. These are not altered by loss of Cln7, indicating no change in pre-synaptic TORC1 activity. Scale bar = 10 µm. The vesicular anti-pS6 staining pattern in the post-synaptic muscle cells is partially reduced in *Cln7*^{84D} mutants. H). Cln7 can be

629 immunoprecipitated in a complex with the TOR activating protein, Rheb. Myc-tagged Cln7
630 and Flag-tagged Rheb proteins were expressed in *Drosophila* S2 cells. I). Western blots for
631 anti-p70 S6K to indicate mTORC1 activity in control of *Cln7*$^{-/-}$ mouse embryonic fibroblasts.
632 Cells were starved of serum, amino acids and glucose for 18 h then insulin, glucose or amino
633 acids returned. Insulin is sufficient to activate mTORC1 but all three are required for full
634 activation. In *Cln7*$^{-/-}$ cells, mTORC1 activity is not activated. Anti-actin was used as a loading
635 control.
636
637
638